Int J Adv Manuf Technol (2002) 20:631–638


The International Journal of
Advanced
Manufacturing
Technology

# Improved Dynamic Cutting Force Model in Peripheral Milling Part I: Theoretical Model and Simulation

X.-W. Liu, K. Cheng, D. Webb and X.-C. Luo
School of Engineering, Leeds Metropolitan University, Leeds, UK

*The accurate prediction of cutting forces is important in controlling the tool deflection and the machining accuracy. In this paper, the authors present an improved theoretical dynamic cutting-force model for peripheral milling with helical end-mills. The theoretical model is based on the oblique cutting principle and includes the size effect of undeformed chip thickness and the influence of the effective rake angle. A set of closed-form analytical expressions is presented. Using the cutting forces measured by Yucesan [1] in tests on a titanium alloy, the cutting-force coefficients are estimated and the cutting-force model verified by simulation. The simulation results indicate that the improved dynamic cutting-force model does predict the cutting forces in peripheral milling accurately. Simulation results for a number of particular examples are presented.*

**Keywords:** Cutting force; Dynamic; Prediction; Peripheral milling; Size effect

## 1. Introduction

Peripheral milling operations are widely used in the automobile, aerospace, textile machinery and other manufacturing industries, where 2D contour parts, i.e. engine components, cams, etc., are milled using complex end-mills. In recent years, due to the need to improve dimensional accuracy of the parts, there has been a push toward reducing the machining errors commonly generated in the milling process. These errors derive from the machine tools, the cutters, the NC programming and the machining process. The errors of the machining process generated in peripheral milling originate from a number of sources, such as tool deflection, workpiece deflection, tool wear, friction, tool run-out, and chatter vibration. Of these, tool deflection due to cutting force is a major problem for precision machining [2].

*Correspondence and offprint requests to*: Prof K. Cheng, School of Engineering, Leeds Metropolitan University, City Campus, Calverley Street, Leeds LS1 3HE, UK. E-mail: k.cheng@lmu.ac.uk

An accurate dynamic cutting-force model is vital for the precise prediction of tool and workpiece deflection in peripheral milling. Several models based on theoretical assumptions and experimental observations have been developed to predict the cutting forces and were reviewed by Smith and Tlusty [3]. Elbestawi [4] and Ismail [5] presented cutting-force models which are formulated from the tangential and radial cutting forces of orthogonal cutting given by [6]

$$F_t = K_s b t \tag{1}$$

$$F_r = c F_t \tag{2}$$

where $K_s$ is the unknown cutting-force coefficient, $b$ is the width of cut, $t$ is the undeformed chip thickness, and $c$ is the cutting-force ratio. Their formulation was confirmed by cutting tests of aluminium. Kolarits [7] and Montgomery [8] also presented cutting-force models which originated from the fundamental theory. Bayoumi [9] and Yucesan [1], however, have developed models from the differential normal and friction forces acting on the rake face given by

$$\mathrm{d}F_n = K_n(\varphi, \theta) A(\theta) \mathbf{n}(\varphi) \mathrm{d}A_v \tag{3}$$

$$\mathrm{d}F_f = K_n(\varphi, \theta) K_f(\varphi, \theta) A(\theta) \mathbf{T}_c(\varphi) \mathrm{d}A_v \tag{4}$$

where $K_n(\varphi, \theta)$ is the unknown pressure coefficient, $K_f(\varphi, \theta)$ is the unknown friction coefficient at the cutting surface–chip interface, $\varphi$ is the position angle of a point on the cutting edge, $\theta$ is the rotation angle of the cutter, $\mathrm{d}A_v$ is the differential area of the undeformed chip cross-section, and $A(\theta)$ is a transformation matrix that rotates the cutter. Altintas [10] and Budak [11] deduced their cutting-force models from the differential tangential, radial and axial cutting forces given by

$$\mathrm{d}F_{ti}(\theta, z) = [K_{te} + K_{tc} t_i(\theta, z)] \mathrm{d}z \tag{5}$$

$$\mathrm{d}F_{ri}(\theta, z) = [K_{re} + K_{rc} t_i(\theta, z)] \mathrm{d}z \tag{6}$$

$$\mathrm{d}F_{ai}(\theta, z) = [K_{ae} + K_{ac} t_i(\theta, z)] \mathrm{d}z \tag{7}$$

where $t_i(\theta, z)$ is the undeformed chip thickness, and the six unknown $K_{**}$ parameters are referred to as the milling-force coefficients. Ramaraj [12] introduced a cutting-force model of peripheral milling with tapered end-mills, which is based on the differential shear force given by

$$dF_S = \frac{\tau t dl}{\sin\varphi_n \cos\beta} \tag{8}$$

where $\tau$ is the shear strength.

Of these models, those presented by Elbestawi [4] and Ismail [5] originate from orthogonal and oblique cutting theories, which are the theoretical foundations for cutting-force models of peripheral milling. However, their models do not consider the size effect of the undeformed chip thickness and the influence of the effective rake angle, which have significant effects on cutting forces. In this paper, we present an improved dynamic cutting-force model, based on the orthogonal and oblique cutting theories, which includes the size effect of undeformed chip thickness and the influence of the effective rake angle.

The fundamentals related to peripheral milling are presented in Section 2, including the oblique cutting model and the geometric model of peripheral cutting with helical end-mills. A new theoretical dynamic cutting-force model of peripheral milling is presented in Section 3, and an estimation of the cutting-force coefficients from previously measured forces in peripheral milling of a titanium alloy is given in Section 4. In Section 5, predicted cutting forces for the peripheral milling of the titanium alloy, from a series of simulations, are presented.

## 2. Fundamental Principles

There are two basic models which are normally used to describe chip formation in metal cutting [6].

1. *Orthogonal cutting*. This is characterised by a cutting edge which is normal and a chip flow which is parallel to the direction of tool motion.
2. *Oblique cutting*. This is characterised by a cutting face which is inclined by an angle $\beta$ with respect to the direction of tool motion and by an angle $\eta_c$ between the direction of chip flow and the direction of tool motion.

### 2.1 Oblique Cutting Model

In the cutting-force models of peripheral milling, one of the common assumptions, and one of the key points, is that the helical flutes of an end-mill are treated as a combination of a series of oblique cutting-edge segments. An oblique cutting geometric model is illustrated in Fig. 1, and the fundamental principles of oblique cutting are summarised as follows [6].

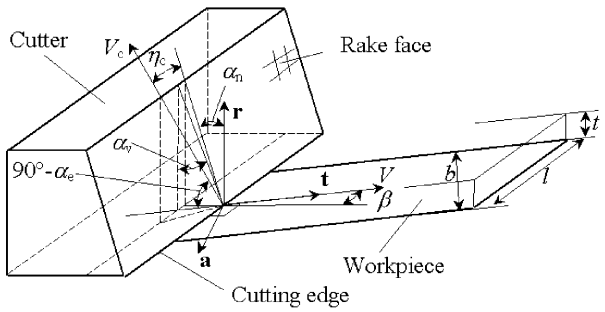


**Fig. 1.** Oblique cutting model.

The relationship between the velocity rake angle and the normal rake angle takes the form

$$\tan\alpha_v = \frac{\tan\alpha_n}{\cos\beta} \tag{9}$$

The effective rake angle, which has an influence on cutting forces, is determined by

$$\sin\alpha_e = \sin\beta \sin\eta_c + \cos\eta_c \cos\beta \sin\alpha_n \tag{10}$$

where the chip flow angle $\eta_c$ may be directly obtained using the following expression:

$$\cos\eta_c = \frac{b_c}{b}\cos\beta \tag{11}$$

When the normal rake angle $\alpha_n$ is equal to or greater than 8°, the chip flow angle $\eta_c$ may be approximately equal to the inclination angle $\beta$ for a variety of tool and work materials, and speeds. This relationship is referred to as Stabler's rule of chip flow [6]. Although Stabler's rule is valid to a first approximation, it has been found that the chip flow angle $\eta_c$ increases relative to the inclination angle $\beta$ when:

1. The normal rake angle $\alpha_n$ decreases.
2. A more efficient cutting fluid is used.
3. The frictional characteristics of the metal-cut are improved.

Equation (10), simplified by use of Stabler's rule, gives:

$$\sin\alpha_e = \sin^2\beta + \cos^2\beta \sin\alpha_n \tag{12}$$

For orthogonal cutting, i.e. $\beta = 0$, the cutting-force components in the power direction and in the undeformed chip thickness direction, become:

$$F_P = ubt \tag{13}$$

$$F_Q = cF_P \tag{14}$$

where the ratio $c$ is commonly about 0.5 [6], $u$ is the total energy per unit volume and is influenced by workpiece material, effective rake angle ($u$ decreases about 1% per degree increase in $\alpha_e$) and undeformed chip thickness. The total energy per unit volume $u$ varies with undeformed chip thickness approximately as:

$$u \sim 1/t^{0.2} \tag{15}$$

This inverse relationship is referred to as the size effect.

Equation (13) is also suitable for oblique cutting, and we can rewrite it as:

$$F_P = uA_v \tag{16}$$

where $A_v = bt = lt\cos\beta$ is the cross-sectional area of the undeformed chip perpendicular to cutting speed.

### 2.2 Geometric Model of Helical End-Mill

The end-mill can be divided into a number of slices along its $z$-direction, as shown in Fig. 2($a$). Within each slice, the cutting action for an individual tooth can be modelled as for single-point oblique cutting, and the tangential and normal cutting forces at any point on the rake face can be obtained from the

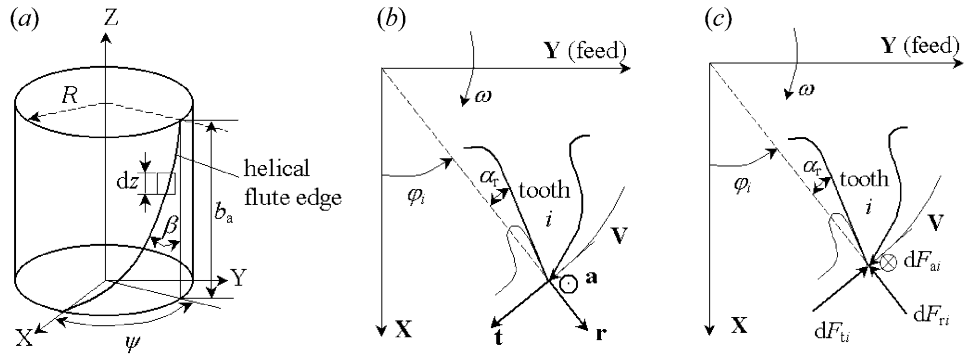


**Fig. 2.** Geometric model: (*a*) helical flute edge geometry; (*b*) curvilinear coordinate system of a tooth element; (*c*) differential cutting force.

oblique cutting model. It is important to note here that the tangential and normal directions together with chip thickness vary during the formation of a single chip in milling. Accordingly, a dynamic model must account for these variations in magnitude and direction of cutting forces.

To relate the helical flute geometry of the end-mill to the tangential cutting force, a curvilinear coordinate system (**t**, **r**, **a**) is established, as shown in Fig. 2(*b*), in which

$$\begin{cases} \mathbf{t} = [\sin(\varphi_i) \ -\cos(\varphi_i) \ 0 \\ \mathbf{r} = \cos(\varphi_i) \ \sin(\varphi_i) \ 0 \\ \mathbf{a} = [0 \quad 0 \quad 1] \end{cases} \tag{17}$$

where

$$\varphi_i = \varphi + \theta + (\mathrm{i} - 1)\frac{2\pi}{m} \quad (1 \le i \le m, \ 0 \le \varphi \le \psi) \tag{18}$$

is the position angle of a point on the cutting edge in the tool coordinate system,

$$\theta = -\omega t_{\mathrm{ime}} \tag{19}$$

is the instantaneous rotation angle of the flute tip from the *x*-axis, $\varphi$ is the helix lag angle, *m* is the flute number of the cutter, $\omega$ is the angular velocity of the spindle, and

$$\psi = \frac{b_a \tan\beta}{R} \tag{20}$$

is the axial immersion angle of a tooth within the axial depth of cut $b_a$.

## 3. Cutting-Force Model

The cutting forces acting on the helical flute's rake face are dependent on the undeformed chip thickness. If d*l* is a portion of the developed cutting edge of elemental length, then d*z* may be considered as the width of an elemental oblique tool with inclination angle $\beta$,

$$\mathrm{d}z = \mathrm{d}l\cos\beta \tag{21}$$

and the differential area of the undeformed chip cross-section

$$\mathrm{d}A_v(\varphi_i) = t_i(\varphi_i)\mathrm{d}z = t_i(\varphi_i)\mathrm{d}l\cos\beta \rightarrow \mathrm{d}l = \frac{R\mathrm{d}\varphi}{\sin\beta} \tag{22}$$

where $t_i(\varphi_i)$ is the undeformed chip thickness.

From Eq. (16) we get the differential tangential cutting force, as shown in Fig. 2(*c*), of the peripheral milling:

$$\mathrm{d}F_{ti}(\varphi_i) = K_s\mathrm{d}A_v(\varphi_i) = K_s t_i(\varphi_i)R\cot\beta\mathrm{d}\varphi \tag{23}$$

where $K_s$ is the tangential cutting-force coefficient, which has the same meaning as the total energy per unit volume *u*. Considering the size effect of undeformed chip thickness and the influence of effective rake angle [6], gives

$$K_s = u_0\left(1 - \frac{\alpha_e - \alpha_{e0}}{100}\right)\left(\frac{t_0}{t_i(\varphi_i)}\right)^{0.2} \tag{24}$$

where $u_0$ is the initial total cutting energy per unit volume, $\alpha_e$ (in degrees) is the effective rake face, $\alpha_{e0}$ (in degrees) is the initial effective rake angle, and $t_0$ is the initial undeformed chip thickness.

From the orthogonal cutting theory, the differential perpendicular cutting force of the peripheral cutting is given by

$$\mathrm{d}F_{ri}(\varphi_i) = c\mathrm{d}F_{ti}(\varphi_i) \tag{25}$$

where the ratio *c* is commonly about 0.3 [5,13,14].

According to the kinematics of milling, the undeformed chip thickness removed by a point on the *i*th helical flute can be calculated as follows [6]:

1. For down-milling, as shown in Fig. 3(*a*):

$$t_i(\varphi_i) = \begin{cases} f_t\sin(\varphi_i) & \text{if } 0 \le \varphi_i \le \Omega \\ 0 & \text{else} \end{cases} \tag{26}$$

2. For up-milling, as shown in Fig. 3(*b*):

$$t_i(\varphi_i) = \begin{cases} f_t\sin(-\varphi_i) & \text{if } -\Omega \le \varphi_i \le 0 \\ 0 & \text{else} \end{cases} \tag{27}$$

where $\Omega$ is the cutter radial immersion angle within the radial depth of cut, and

$$\Omega = \arccos\left(1 - \frac{d}{R}\right) \tag{28}$$

To develop the total force applied on the whole cutter, the differential forces are resolved into the feed (*y*) and normal (*x*) directions. As the differential cutting-force components are just opposite to the corresponding directions of the curvilinear coordinate system (**t**, **r**, **a**), Eqs (23) and (25) become

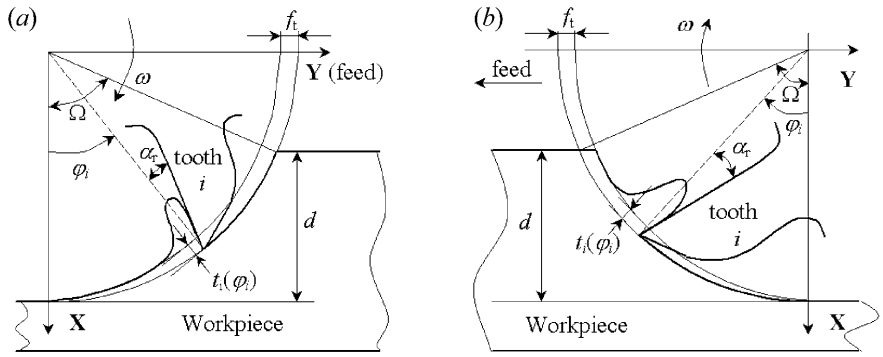


**Fig. 3.** Peripheral milling method: (*a*) down-milling; (*b*) up-milling.

$$\begin{cases} dF_{tix} = -K_s t_i(\varphi_i) R\cot\beta \sin\varphi_i d\varphi \\ dF_{tiy} = K_s t_i(\varphi_i) R\cot\beta \cos\varphi_i d\varphi \end{cases} \tag{29}$$

$$\begin{cases} dF_{rix} = -cK_s t_i(\varphi_i) R\cot\beta \cos\varphi_i d\varphi \\ dF_{riy} = -cK_s t_i(\varphi_i) R\cot\beta \sin\varphi_i d\varphi \end{cases} \tag{30}$$

Summing these two equations gives the differential forces in $x$ and $y$ as:

$$\begin{cases} dF_{ix} = -K_s t_i(\varphi_i) R\cot\beta \ (\sin\varphi_i + c\cos\varphi_i) d\varphi \\ dF_{iy} = K_s t_i(\varphi_i) R\cot\beta \ (\cos\varphi_i - c\sin\varphi_i) d\varphi \end{cases} \tag{31}$$

Letting

$$u' = u_0 \left(1 - \frac{\alpha_e - \alpha_{e0}}{100}\right) \left(\frac{t_0}{f_t}\right)^{0.2} \tag{32}$$

Then the tangential cutting-force coefficient given by Eq. (24) becomes

1. For down-milling:

$$K_s = u'(\sin\varphi_i)^{-0.2} \ (0 \le \varphi_i \le \Omega) \tag{33}$$

2. For up-milling:

$$K_s = u'[\sin(-\varphi_i)]^{-0.2} \ (-\Omega \le \varphi_i \le 0) \tag{34}$$

By applying Eqs (33) and (34), Eq. (31) becomes

1. For down-milling:

$$\begin{cases} dF_{ix} = -u' t_i(\varphi_i) R\cot\beta \ (\sin^{0.8}\varphi_i + c\sin^{-0.2}\varphi_i \cos\varphi_i) d\varphi \\ dF_{iy} = u' t_i(\varphi_i) R\cot\beta \ (\sin^{-0.2}\varphi_i \cos\varphi_i - c\sin^{0.8}\varphi_i) d\varphi \end{cases} \tag{35}$$

2. For up-milling:

$$\begin{cases} dF_{ix} = -u' t_i(\varphi_i) R\cot\beta \ [\sin\varphi_i \sin^{-0.2}(-\varphi_i) \\ \qquad + c\sin^{-0.2}(-\varphi_i)\cos\varphi_i] d\varphi \\ dF_{iy} = u' t_i(\varphi_i) R\cot\beta \ [\sin^{-0.2}(-\varphi_i)\cos\varphi_i \\ \qquad - c\sin\varphi_i \sin^{-0.2}(-\varphi_i)] d\varphi \end{cases} \tag{36}$$

By applying Eq. (26), and noting that $d\varphi_i = d\varphi$, Eq. (35) becomes

$$\begin{cases} dF_{ix} = -u' f_t R\cot\beta \ (\sin^{1.8}\varphi_i + c\sin^{0.8}\varphi_i \cos\varphi_i) d\varphi_i \\ dF_{iy} = u' f_t R\cot\beta \ (\sin^{0.8}\varphi_i \cos\varphi_i - c\sin^{1.8}\varphi_i) d\varphi_i \\ \left(\varphi_i = \varphi - \omega t_{ime} + (i-1)\dfrac{2\pi}{m}\right) \\ \left(0 \le \varphi_i \le \Omega\right) \end{cases} \tag{37}$$

By applying Eq. (27), and noting that $\sin(-\varphi_i) = -\sin\varphi_i$, Eq. (36) becomes

$$\begin{cases} dF_{ix} = u' f_t R\cot\beta \ [\sin^{1.8}(-\varphi_i) - c\sin^{0.8}(-\varphi_i)\cos\varphi_i] d\varphi_i \\ dF_{iy} = u' f_t R\cot\beta \ [\sin^{0.8}(-\varphi_i)\cos\varphi_i + c\sin^{1.8}(-\varphi_i)] d\varphi_i \\ \left(\varphi_i = \varphi - \omega t_{ime} + (i-1)\dfrac{2\pi}{m}\right) \\ \left(-\Omega \le \varphi_i \le 0\right) \end{cases} \tag{38}$$

Let $\xi_i = -\varphi_i$, as $\cos(-\varphi_i) = \cos\varphi_i$ and $d\xi_i = -d\varphi_i$, Eq. (38) becomes

$$\begin{cases} dF_{ix} = -u' f_t R\cot\beta \ [\sin^{1.8}(\xi_i) - c\sin^{0.8}(\xi_i)\cos\xi_i] d\xi_i \\ dF_{iy} = -u' f_t R\cot\beta \ [\sin^{0.8}(\xi_i)\cos\xi_i + c\sin^{1.8}(\xi_i)] d\xi_i \\ \left(\xi_i = -\varphi + \omega t_{ime} - (i-1)\dfrac{2\pi}{m}\right) \\ \left(0 \le \xi_i \le \Omega\right) \end{cases} \tag{39}$$

where ($1 \le i \le m$, $0 \le \varphi \le \psi$).

The total cutting force applied on the whole cutting edge is given by

$$\begin{cases} F_{ix} = \displaystyle\int_{\varphi_s}^{\varphi_e} dF_{ix} d\varphi_i \\ F_{iy} = \displaystyle\int_{\varphi_s}^{\varphi_e} dF_{iy} d\varphi_i \end{cases} \quad \text{or} \quad \begin{cases} F_{ix} = \displaystyle\int_{\xi_s}^{\xi_e} dF_{ix} d\xi_i \\ F_{iy} = \displaystyle\int_{\xi_s}^{\xi_e} dF_{iy} d\xi_i \end{cases} \tag{40}$$

where $\varphi_s$ ($\xi_s$) and $\varphi_e$ ($\xi_e$) are the lag angular locations of the start- and endpoints of contact of the cutting edge, and are defined in the following kinematics analysis.

Integrating between the extreme values of the parametric angle $\varphi_s$ ($\xi_s$) and $\varphi_e$ ($\xi_e$) gives the total cutting force applied on the $i$th tooth.

1. For down-milling:

$$\begin{cases} F_{ix} \approx -u' f_t R\cot\beta \ (0.5\varphi_i - 0.25\sin 2\varphi_i + 0.5556\, c\sin^{1.8}\varphi_i)\Big|_{\varphi_s}^{\varphi_e} \\ F_{iy} \approx u' f_t R\cot\beta \ (0.5556\sin^{1.8}\varphi_i - 0.5\, c\varphi_i + 0.25\, c\sin 2\varphi_i)\Big|_{\varphi_s}^{\varphi_e} \end{cases} \tag{41}$$

Because $0 \le \varphi \le \psi$, $\varphi_i = \varphi - \omega t_{\text{ime}} + (i-1)\,2\pi/m$ and $0 \le \varphi_i \le \Omega$ gives the extreme values of the parametric angle $\varphi_i$ as

$$\varphi_s = \max\left(0, -\omega t_{\text{ime}} + (i-1)\frac{2\pi}{m}\right) \tag{42}$$

$$\varphi_e = \min\left(\Omega, \psi - \omega t_{\text{ime}} + (i-1)\frac{2\pi}{m}\right) \tag{43}$$

2. For up-milling:

$$\begin{cases} F_{ix} \approx -u' f_t R\cot\beta(0.5\xi_i - 0.25\sin 2\xi_i - 0.5556\, c \sin^{1.8}\xi_i)\Big|_{\xi_s}^{\xi_e} \\ F_{iy} \approx -u' f_t R\cot\beta\,(0.5556\sin^{1.8}\xi_i + 0.5\, c\xi_i - 0.25\, c\sin 2\xi_i)\Big|_{\xi_s}^{\xi_e} \end{cases} \tag{44}$$

Also, $\xi_i = -\varphi + \omega t_{\text{ime}} - (i-1)\,2\pi/m$ and $0 \le \xi_i \le \Omega$ gives the extreme values of the parametric angle $\xi_i$ as

$$\xi_s = \max\left(0, -\psi + \omega t_{\text{ime}} - (i-1)\frac{2\pi}{m}\right) \tag{45}$$

$$\xi_e = \min\left(\Omega, \omega t_{\text{ime}} - (i-1)\frac{2\pi}{m}\right) \tag{46}$$

Summing up the cutting forces acting on all the $m$ helical flutes gives the total force applied on the whole cutter:

$$\begin{cases} F_x = \sum_{i=1}^{m} F_{ix} \\ F_y = \sum_{i=1}^{m} F_{iy} \end{cases} \tag{47}$$

## 4. Estimation of Cutting-Force Coefficients

Equations (41) and (44) are closed-form analytical expressions with the following two coefficients to be estimated by experiment:

1. $u_0$, the initial total cutting energy per unit volume, under the initial cutting condition $\alpha_{e0} = 0°$ and $t_0 = 0.25$ mm [6]
2. $c$, the cutting-force ratio.

$u_0$ is dependent on workpiece material, cutter material, cutting-edge radius, friction characteristics between the workpiece and the cutter (no cutting fluid, continuous chip and no built-up edge are assumed). The ratio $c$ is about 0.3 [13,14] to 0.5 [10], and depends mainly on the cutter geometry.

In order to obtain values for the coefficients, some previously measured cutting forces are considered. Yucesan and Altintas [1] have presented a detailed description of their experimentally measured cutting forces in the peripheral milling of a titanium alloy. These experimental results were used to verify a different cutting-force model, and it is appropriate to use them to verify our improved cutting-force model.

For consistency, we choose the same cutter, workpiece material and cutting conditions (for our simulation) as in the cutting tests conducted by Yucesan and Altintas. These are:

1. Cutter: a single-fluted carbide end-mill with a helix angle $\beta = 30°$, a rake angle $\alpha_r = 12°$ and a diameter of 19.06 mm.
2. Material properties of the carbide cutter: 90% WC, 10% Co, hardness 92 Rockwell.
3. Material properties of the titanium alloy: 6% Al, 4% V, Young's modulus = 110 GPa, Poisson's ratio = 0.34, tensile strength = 900 Mpa.
4. Cutting parameters: axial depth of cut $b_a = 7.62$ mm, radial depth of cut $d = 19.06$ mm (slotting), $\psi = 26.45°$, $\Omega = \pi$, spindle rotation speed $n = 500$ rpm (cutting speed $V = 498.99$ mm s$^{-1}$), with a feedrate ranging from 0.0127 mm per tooth to 0.2030 mm per tooth. The cutting forces measured by Yucesan [1] are shown in Fig. 4.

We also assume the conditions presented by Shaw [6], i.e. that the initial total cutting energy per unit volume $u_0 = 3.51 \times 10^9\ J\ m^{-3}$, the initial effective rake angle $\alpha_{e0} = 0°$, the initial undeformed chip thickness $t_0 = 0.25$mm, and the cutting-force ratio $c = 0.5$. With these assumed values the instantaneous predicted forces were found to have the same shape as shown in Fig. 4, but with different amplitudes. Adjusting the initial total cutting energy per unit volume and the cutting-force ratio to $u_0 = 2.0 \times 10^9$ J m$^{-3}$, $c = 0.45$, the instantaneous predicted forces shown in Fig. 5 are obtained. Comparing these results to the measured cutting forces illustrated in Fig. 4, it is found that there is very good agreement.

From Fig. 5 it can be seen that, when the feedrate is larger than 0.0254 mm per tooth, the predicted cutting forces are very good approximations to the measured cutting forces and the improved dynamic cutting-force model can be used to predict the cutting forces accurately. However, when the feedrate is smaller than 0.0254 mm per tooth, the predicted cutting forces are smaller than the measured values. This result reveals that when the feedrate is far smaller than the radius of the cutting edge, the ploughing force is dominant [15] and the cutting-force model must be modified.

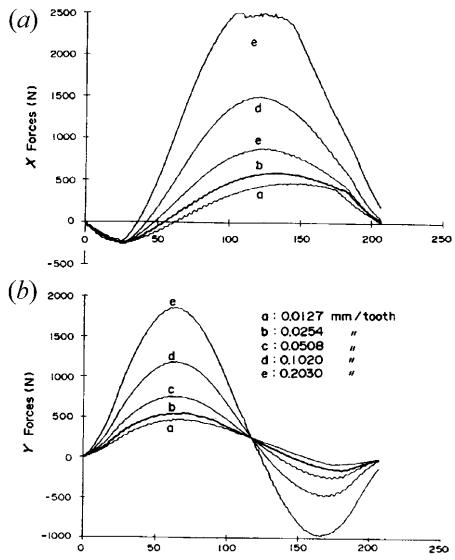


**Fig. 4.** Measured cutting forces at various feedrates (Yucesan [1]).

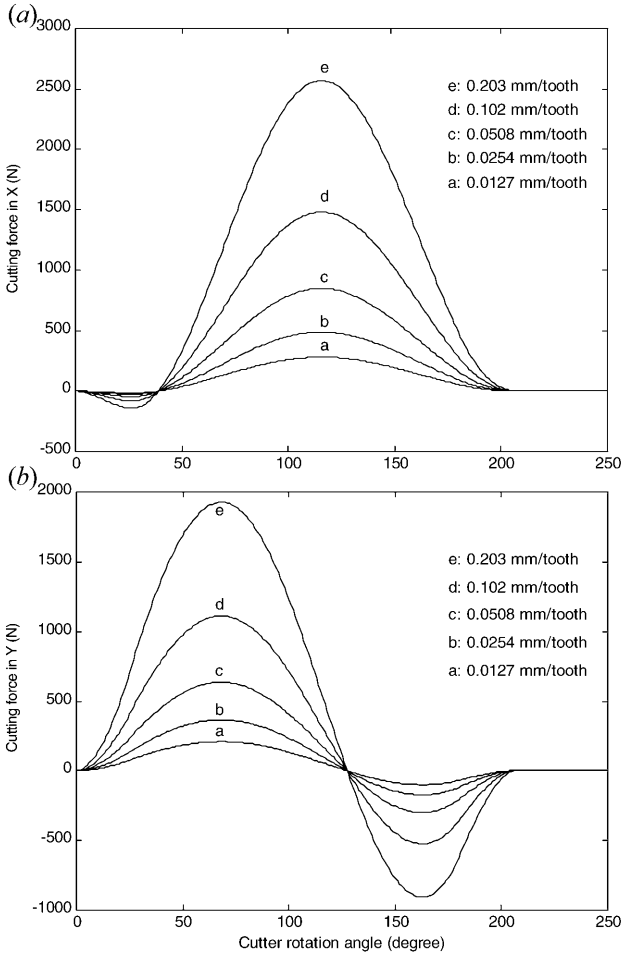


**Fig. 5.** Predicted cutting forces for a full immersion up-milling test ($m$ = 1, $\alpha_r$ = 12°, $b_a$ = 7.62 *mm*, $d$ = 19.06 *mm*, $\psi$ = 26.45°, $u_0$ = 2 × $10^9$ *J* $m^{-3}$).

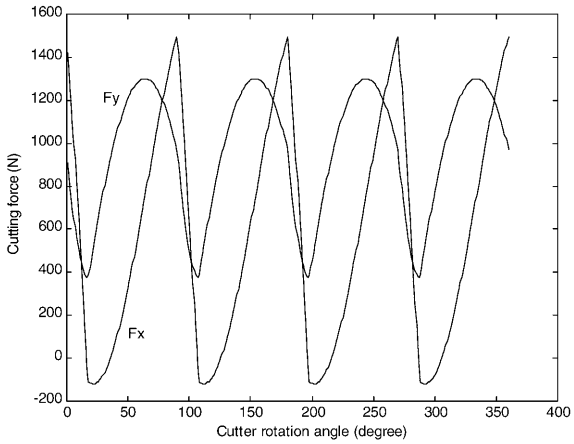


**Fig. 6.** Predicted cutting forces for a half immersion up-milling test ($m$ = 4, $f_t$ = 0.203 mm per tooth, $\alpha_r$ = 12 °, $b_a$ = 5.08 mm, $d$ = 9.525 mm).

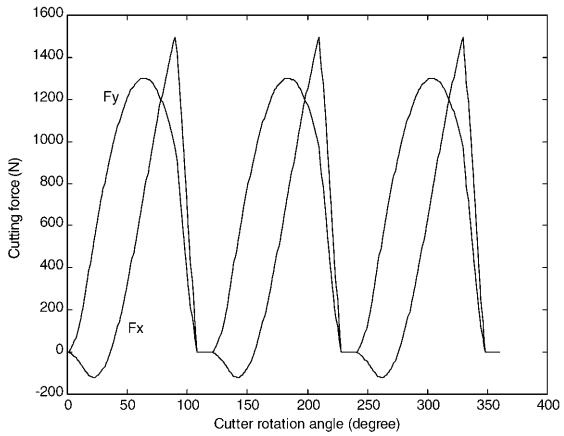


**Fig. 7.** Predicted cutting forces for a half immersion up-milling test ($m$ = 3).

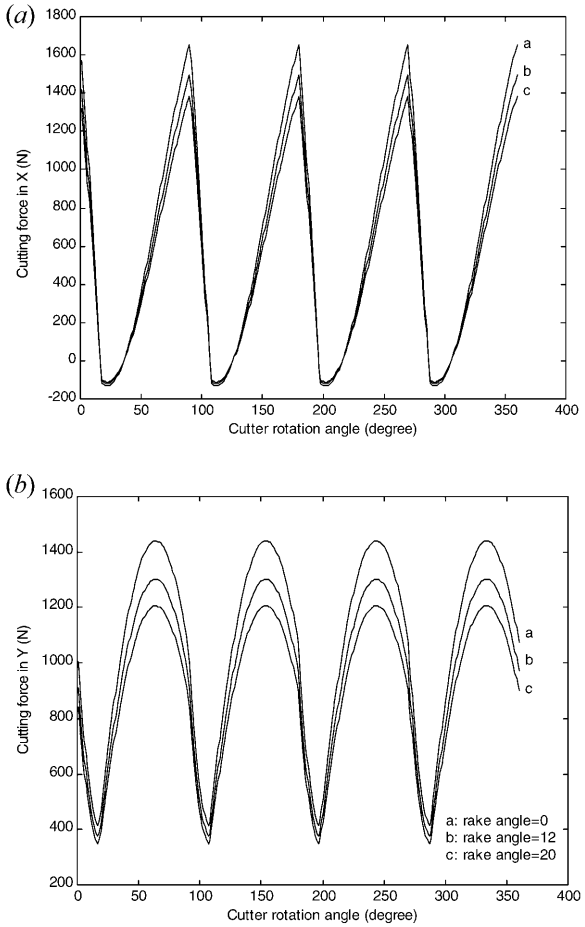


**Fig. 8.** Influence of rake angle on the cutting forces ($m$ = 4, $f_t$ = 0.203 mm per tooth, $b_a$ = 5.08 mm, $d$ = 9.525 mm). (rake angle in °.)

## 5. Cutting-Force Simulation

A series of cutting simulations on the titanium alloy were carried out for three- and four-fluted carbide end-mills (with a

common helix angle of $\beta = 30°$ and a diameter of 19.06 mm) at a constant spindle rotation speed of 500 rpm. (The cutting speed is constant at $V = 498.99$ mm $s^{-1}$.)

Figure 6 shows instantaneous predicted cutting forces for a flute number $m = 4$, a feedrate $f_t = 0.203$ mm per tooth, an axial depth of cut $b_a = 5.08$ mm ($\psi = 17.63°$), and an radial depth of cut $d = 9.525$ mm ($\Omega = 89.97°$). The variation in $F_x$ shows that, when the cut-in process of each tooth starts (as the second tooth cuts out), $F_x$ reaches a maximum value of about 1500 N; and when the cut-in process ends, the maximum negative value of $F_x$ is about $-140$ N. This force variation will greatly influence the surface form accuracy of the finished part.

Figure 7 shows predicted values of cutting force for the same condition but for a flute number $m = 3$. The variation in $F_x$ shows that during the cut-in process of each tooth, $F_x$ has small negative values, changes from 0 to $-101$ N. The force variation will have much smaller influence on the surface form accuracy of the finished part. This result implies the possibility of reducing the surface form error due to tool deflection through carefully selecting the flute number of the cutter.

Figure 8 shows the predicted cutting forces when the rake angle $\alpha_r$ changes. The only difference is the amplitude of the cutting forces.

Figure 9 shows the predicted cutting forces when the feedrate $f_t$ changes. It is worth noticing that, when $f_t = 0.102$ mm per tooth, the maximum value of $F_x$ is greater than the half maximum value as $f_t = 0.203$ mm per tooth, due to the size effect of undeformed chip thickness.

Figure 10 shows the influence of the radial depth of cut on the cutting forces. A very interesting fact is that during the cut-in process of each tooth, when the radial depth of cut changes, $F_x$ changes significantly. When $d = 6.8$ mm, the force variation will have a much smaller influence on the surface form accuracy of the finished part. This result implies the possibility of reducing the surface form error due to tool deflection through carefully selecting the radial depth of cut.

It is worth mentioning that Fuh [16] developed a second-order model utilising response surface methodology (RSM) to model the dimensional accuracy for peripheral milling, and reported that the peripheral milling accuracy is generally reduced with increased value of radial depth of cut. The model did not consider the influence of the cutting-force distribution on the dimensional accuracy. The simulation results shown in Fig. 10 indicate that the dimensional accuracy depends not only on the value of the radial depth of cut but also on the influence on the cutting-force distribution of the radial depth of cut.

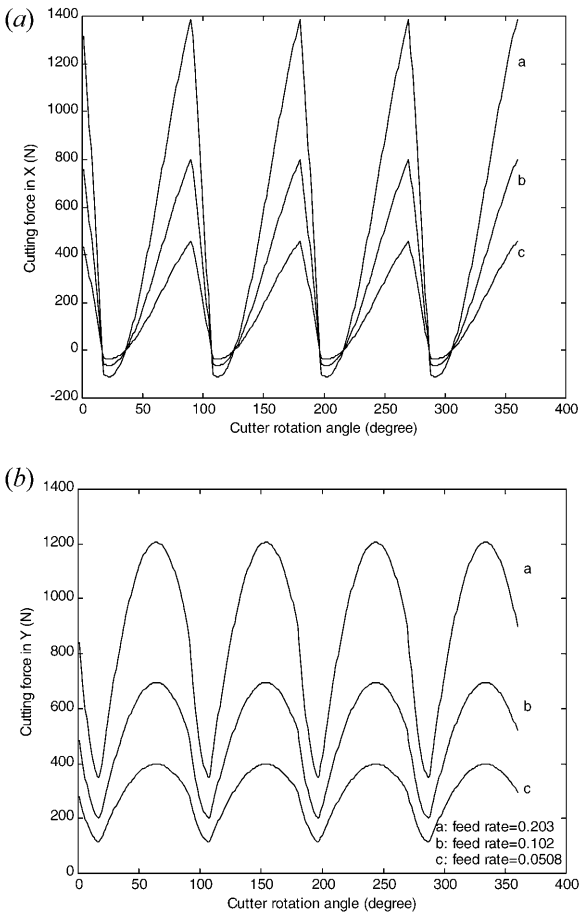


**Fig. 9.** Influence of feedrate on the cutting forces ($m$ = 4, $\alpha_r$ = 20°, $b_a$ = 5.08 mm, $d$ = 9.525 mm). (feedrate in mm per tooth.)

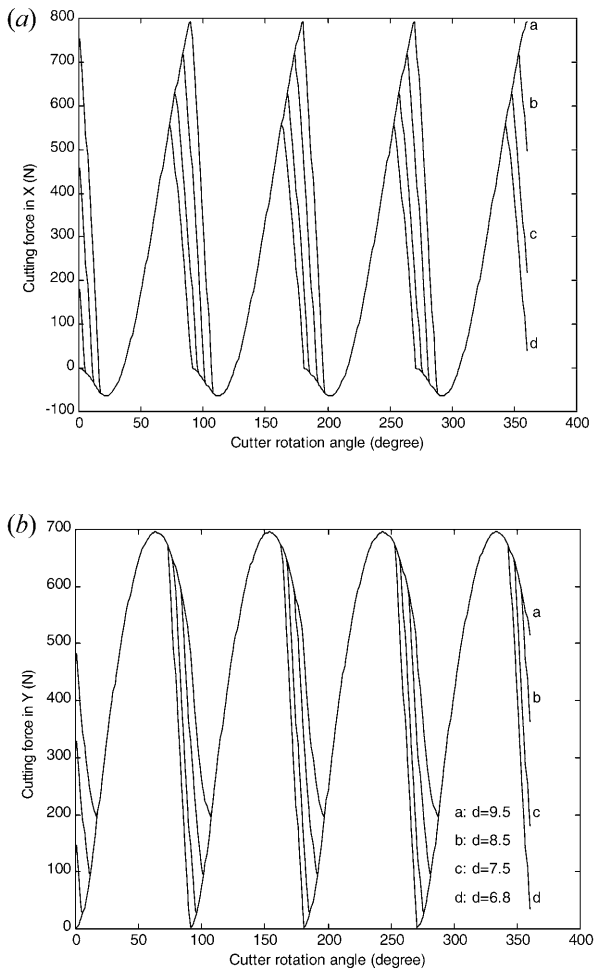


**Fig. 10.** Influence of radial depth of cut on the cutting forces ($m$ = 4, $\alpha_r$ = 20°, $b_a$ = 5.08 mm, $f_t$ = 0.102 mm per tooth). ($d$ in mm.)

## 6. Conclusions

The research presented here reinforces the size effect of undeformed chip thickness and the influence of the effective rake angle in peripheral milling. The improved theoretical dynamic cutting-force model presented simple closed form analytical expression. Verification results indicate that the model is suitable for general peripheral milling, when the feedrate is larger than the radius of the cutting edge. For fine milling, when the feedrate is smaller than the radius of the cutting edge, the measured cutting force will be greater than the cutting force predicted by the model. This result reveals that the ploughing force is dominant in this condition and the general cutting force model is no longer effective. Case studies reveal that the model may be very effective in reducing the surface form error due to tool deflection if the flute number, the axial depth of cut and the radial depth of cut are selected carefully.

*Acknowledgements*

This work is supported by the Engineering and Physical Sciences Research Council (EPSRC) with the grant GR/R13395.

### References

1. G. B. Yucesan and Y. Altintas, "Improved modelling of cutting force coefficients in peripheral milling", International Journal of Machine Tools and Manufacture, 34(4), pp. 473–487, 1994.
2. J. W. Sutherland and R. E. Devor, "An improved method for cutting force and surface error prediction in flexible end milling systems", Transactions ASME, Journal of Engineering for Industry, 108, pp. 269–279, 1986.
3. S. Smith and J. Tlusty, "An overview of modeling and simulation of the milling process", Transactions ASME, Journal of Engineering for Industry, 113, pp. 169–175, 1991.
4. M. A. Elbestawi, F. Ismail, R. Du and B. C. Ullagaddi, "Modelling machining dynamics including damping in the tool-workpiece interface", Transactions ASME, Journal of Engineering for Industry, 116, pp. 435–439, 1994.
5. F. Ismail, M. A. Elbestawi, R. Du and K. Urbasik, "Generation of milled surface including tool dynamics and wear", Transactions ASME, Journal of Engineering for Industry, 115, pp. 245–252, 1993.
6. M. C. Shaw, Metal Cutting Principles, Oxford University Press, Oxford, 1984.
7. F. M. Kolarits and W. R. DeVries, "A mechanistic dynamic model of end milling for process controller simiulation", Transactions ASME, Journal of Engineering for Industry, 113, pp. 176–183, 1991.
8. D. Montgomery and Y. Altintas, "Mechanism of cutting force and surface generation in dynamic milling", Transactions ASME, Journal of Engineering for Industry, 113, pp. 160–168, 1991.
9. A. E. Bayoumi, G. Yucesan and L. A. Kendall, "An analytic mechanistic cutting force model for milling operations: a theory and methodology", Transactions ASME, Journal of Engineering for Industry, 116, pp. 324–339, 1994.
10. Y. Altintas and P. Lee, "Mechanics and dynamics of ball end milling", Transactions ASME, Journal of Engineering for Industry, 120(4), pp. 684–692, 1998.
11. E. Budak, Y. Altintas and E. J. A. Armarego, "Prediction of milling force coefficients from orthogonal cutting data", Transactions ASME, Journal of Manufacturing Science and Engineering, 118(2), pp. 216–224, 1996.
12. T. C. Ramaraj and E. Eleftheriou, "Analysis of the mechanics of machining with tapered end milling cutters", Transactions ASME, Journal of Engineering for Industry, 116, pp. 398–404, 1994.
13. J. Tlusty, "Machine dynamics", in R. I. King, ed., Handbook of High Speed Machining Technology, Chapman and Hall, New York, pp. 48–153, 1985.
14. J. Tlusty and P. Macneil, "Dynamics of cutting forces in end milling," Annals CIRP, 24(1), pp. 21–25, 1975.
15. D. J. Waldorf, R. E. DeVor and S. G. Kapoor, "An evaluation of ploughing models for orthogonal machining", Transactions ASME, Journal of Manufacturing Science and Engineering, 121(4), pp. 550–558, 1999.
16. K.-H. Fuh and H.-Y. Chang, "An accuracy model for the peripheral milling of aluminium alloys using response surface design", Journal of Materials Processing Technology, 72(1), pp. 42–47, 1997.

### Nomenclature

| | |
|---|---|
| $\Omega$ | radial immersion angle |
| $\alpha_e$ | effective rake angle |
| $\alpha_{e0}$ | initial effective rake angle |
| $\alpha_n$ | normal rake angle |
| $\alpha_r$ | radial rake angle, equivalent to $\alpha_v$ in oblique cutting |
| $\alpha_v$ | velocity rake angle |
| $\beta$ | helix angle of end-mill, inclination angle of oblique cutting |
| $\theta$ | tool rotation angle |
| $\varphi$ | helix lag angle |
| $\varphi_s$, $\varphi_e$ | helix lag angular locations of the starting and ending points of contact |
| $\varphi_i$ | position angle of a point on the cutting edge of the $i$th helical flute |
| $\psi$ | axial immersion angle of a tooth within $b_a$ |
| $\omega$ | spindle rotation angle speed |
| $\eta_c$ | chip flow angle |
| $A_v$, $dA_v$ | cross-sectional area of undeformed chip perpendicular cutting speed |
| $F_P$, $F_Q$ | cutting-force components in power direction and undeformed chip thickness direction |
| $dF_{ti}$, $dF_{ri}$ | differential cutting-force components of the $i$th helical flute in tangential and radial directions |
| $dF_{ix}$, $dF_{iy}$ | differential cutting-force components of the $i$th helical flute in $x$ and $y$ directions |
| $F_{ix}$, $F_{iy}$ | total cutting-force components of the $i$th helical flute in $x$ and $y$ directions |
| $F_x$, $F_y$ | total cutting-force components in $x$ and $y$ directions |
| $K_s$ | tangential cutting-force coefficient |
| $R$ | tool radius |
| $V$ | cutting speed |
| $V_c$ | chip speed |
| $b_a$ | axial depth of cut (peripheral milling) |
| $b$ | width of cut (oblique cutting) |
| $b_c$ | width of chip (oblique cutting) |
| $c$ | cutting-force ratio |
| $d$ | radial depth of cut (peripheral milling) |
| $f_t$ | feed per tooth per revolution |
| $m$ | number of cutter flutes |
| $n$ | spindle rotation speed (rpm) |
| $t_{ime}$ | time |
| $t$ | undeformed chip thickness |
| $t_i(\varphi_i)$ | undeformed chip thickness of the $i$th tooth in angle position $\varphi_i$ |
| $t_0$ | initial undeformed chip thickness |
| $t_c$ | chip thickness |
| $u$ | total cutting energy per unit volume |
| $u_0$ | initial total cutting energy per unit volume |
| $\mathbf{t}$, $\mathbf{r}$, $\mathbf{a}$ | unit vectors defining the curvilinear coordinate system along the cutting edge |